AD-A184 686 INDENTATION DAMAGE IN CERAMICS(U) NATIONAL BUREAU OF STANDARDS GAITHERSBURG MD CERAMICS DIV B R LAWN ET AL 30 MAY 87 ARO-215221 3-MS MIPR-ARO-124-86 1/1

UNCLASSIFIED F/G 11/2 NL

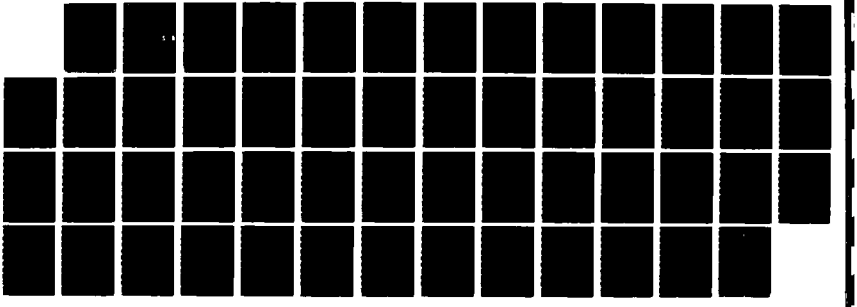

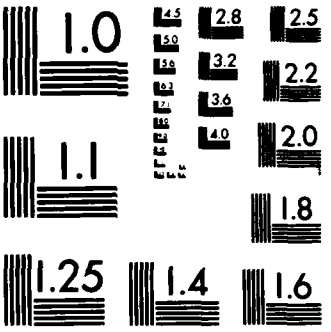

MICROCOPY RESOLUTION TEST CHART
NATIONAL BUREAU OF STANDARDS-1963-A

INDENTATION DAMAGE IN CERAMICS

FINAL REPORT

B. R. LAWN AND B. J. HOCKEY

March 1985 to March 1987

U. S. ARMY RESEARCH OFFICE

CONTRACT/GRANT NUMBER: MIPR ARO 124-86

NATIONAL BUREAU OF STANDARDS
CERAMICS DIVISION
GAITHERSBURG, MD 20899

INDENTATION DAMAGE IN CERAMICS

A. STATEMENT OF PROBLEM STUDIED

The basic processes of indentation damage in brittle ceramics have been studied. Attention has focussed on the roles of material crystallography and microstructure in determining the nature of the damage pattern. Microscopy techniques, particularly transmission electron microscopy, have been used to characterize the attendant deformation and fracture at Vickers indentation sites. Strength, toughness, and wear measurements have been carried out on polycrystalline materials to ascertain how the damage characteristics influence the ensuing mechanical properties. It is concluded that material microstructure can be a crucial factor in structural design with ceramics.

B. SUMMARY OF IMPORTANT RESULTS

Nature of Indentation Damage

Transmission electron microscopy studies have been made on selected brittle ceramic materials, namely silicon, sapphire and silicon carbide. We have established that the deformation mechanisms are of a kind different from that of classical dislocation glide. In silicon, for instance, we have found evidence for amorphization of the crystal structure in the central regions of the indentation sites. This work is currently being prepared for publication. (Reference 3, Publications List). We have also identified twins, especially in sapphire. However, the predominant deformation mechanism in all these materials is a high-stress, shear-activated catastrophic slip process (somewhat akin to shear faulting in earthquakes).

The importance of the deformation modes is that they act as precursors to cracking. There are strong rate effects associated with this attendant cracking; e.g. high-rate (impact) contacts suppress cracking. We intend to explore this phenomenon in greater detail at a later date.

Microstructure Strength Properties

Work has also been carried out on the interrelations between the microstructural makeup and the strength and toughness properties of ceramics. Much of this work has focussed on alumina and glass ceramics. Thus, although we may regard alumina as a simple polycrystalline form of sapphire, we find that the presence of grain boundaries can have a profound effect on the way that indentation cracks (or any cracks, for that matter) propagate to failure. In particular, we find that the cracks are "bridged" by interlocking grains behind the advancing crack tip. Thus bridging, we now believe, is the principal cause of toughening in nontransforming ceramics.

Accordingly, we have extensively analyzed the strength data in terms of a specific bridging model developed by our group. The results of this work are summarized in Reference 1, Publications List.

Wear Properties

As an adjunct to the microstructural effects above, we have examined the wear properties of the same alumina ceramics investigated in the strength studies. In particular, we have measured the grinding resistance of these materials. We find some apparently remarkable results. Whereas all the conventional theories of wear and erosion predict that grinding resistance should scale with toughness, we find just the opposite. This threatens the

entire basis of materials selection for maximum damage resistance of ceramic components. The reason for the discrepancy lies in the fact that the conventional toughness measures the resistance to the growth of large-scale cracks, whereas grinding and wear takes place on the microscale. Again, the bridging mechanism referred to in the previous section is invoked to explain the results.

This work is summarized as Reference 2, Publications List.

C. PUBLICATIONS LIST

1. "Crack Resistance by Interfacial Bridging: Its Role in Determining Strength Characteristics"
   R.F. Cook, C.J. Fairbanks, B.R. Lawn, Y-W. Mai
   J. Mater. Research, in press.

2. "Microstructural Effects on Grinding of Alumina and Glass Ceramics"
   D.B. Marshall, B.R. Lawn, R.F. Cook
   J. Amer. Ceram. Soc., in press.

3. "Indentation Damage in Silicon"
   D.R. Clarke and B.J. Hockey
   In preparation

D. PARTICIPATING PERSONNEL

B.R. Lawn
B.J. Hockey
] Co-principal Investigators

E. APPENDED PUBLICATIONS

Crack Resistance By Interfacial Bridging : Its Role in Determining Strength Characteristics

Robert F. Cook

IBM

Thomas J. Watson Research Center

Yorktown Heights, NY. 10598

Carolyn J. Fairbanks, Brian R. Lawn, Yiu-Wing Mai*

Ceramics Division

National Bureau of Standards

Gaithersburg, MD. 20899

---

* On leave from the Department of Mechanical Engineering, University of Sydney, N.S.W. 2006, Australia

Abstract

An indentation-strength formulation is presented for nontransforming ceramic materials which show an increasing toughness with crack length (T-curve, or R-curve) due to the restraining action of interfacial bridges behind the crack tip. By assuming a stress-separation function for the bridges a microstructure-associated stress intensity factor is determined for the penny-like indentation cracks. This stress intensity factor opposes that associated with the applied loading, thereby contributing to an apparent toughening of the material, ie the measured toughness in excess of that associated with the intrinsic cohesion of the grain boundaries (intergranular fracture). The incorporation of this additional factor into conventional indentation fracture mechanics allows the strengths of specimens with Vickers flaws to be calculated as a function of indentation load. The resulting formulation is used to analyze earlier indentation-strength data on a range of alumina, glass-ceramic and barium titanate materials. Numerical deconvolution of these data determines the appropriate T-curves. A feature of the analysis is that materials with pronounced T-curves have the qualities of flaw tolerance and enhanced crack stability. It is suggested that the indentation-strength methodology, in combination with the bridging model, can be a powerful tool for the development and characterization of structural ceramics, particularly with regard to grain boundary structure.

1 Introduction

Recent studies have shown that many polycrystalline, non-phase-transforming ceramics exhibit an increasing resistance to crack propagation with crack length.[1-8] At small flaw sizes, comparable to the scale of the microstructure, the toughness, T, is an intrinsic quantity representative of the weakest fracture path. At large flaw sizes the toughness tends to a higher, steady-state value representative of the cumulative crack/microstructure interactions in the polycrystal. The progressive transition from the low to high toughness limits during crack extension is described as the T-curve. *

Perhaps the most comprehensive studies of this T-curve behavior have been made using a controlled flaw technique,[1-4] in which the strengths of specimens containing indentations are measured as a function of indentation load. It was found that, for large flaws, the strengths tend to an "ideal" -1/3 power law dependence of strength on indentation load, indicative of a non-varying toughness. At small flaw sizes, however, the strengths decrease markedly from this ideal behavior, tending instead to a load-independent plateau. Significantly, in a group of polycrystalline alumina materials it was found that the strengths at large flaw sizes were all greater than those of single crystal sapphire whereas the reverse tended to be true at small flaw sizes.[1] Taken with the observation that the fracture in these aluminas is intergranular these results suggest that the grain boundaries are paths of weakness, but that there is some mechanism operating which more than compensates for this intrinsic weakness

---

* The concepts of T-curve and R-curve are equivalent.[9] In the former the equilibrium condition is obtained by equating the net stress intensity factor, K, characterizing the net applied load on the crack, to the toughness T (alternatively designated K_{IC} in some of the earlier literature) characterizing critical crack resistance forces. In the latter, the mechanical energy release rate, G, derived from the work done by the applied loading during crack extension, is equated to the energy necessary to create the fracture surfaces, R.

as the flaw size increases. Moreover, the strength-load responses of the polycrystalline materials themselves, even those with similar grain sizes, tended to cross each other.[1] It would appear that the nature of the grain boundary, as well as the grain size, influences the fracture behavior.

Two other sets of experiments provide vital clues as to the mechanism of crack/microstructure interaction underlying the T-curve behavior. In the first set, Knehans and Steinbrech[6] propagated large cracks in alumina using the single-edge-notched beam geometry. They observed strongly rising T-curves as cracks propagated from the tip of the notch. However, when interfacial material was removed from behind the crack tip by careful sawing, the toughness did not continue up the T-curve but reverted to its original level, implying that the critical mechanism must be operating in the "wake" of the crack tip. In the second set of experiments, Swanson et al[8] observed crack propagation in alumina using both indented-disk and tapered-cantilever beam specimens. Active grain-localized "bridges" were observed at the primary crack interface, over a "zone length" of millimeter scale. The implication here is that interfacial bridging ligaments behind the tip are providing a restraining influence on crack extension. The reversion to the base of the T-curve in the experiments of Knehans and Steinbrech may be interpreted in terms of the removal of these restraining ligaments.

Mai and Lawn[10] developed a fracture mechanics model for the propagation of ligamentary bridged cracks, incorporating parameters characterizing the inter-bridge spacing, the intrinsic intergranular toughness, and the force-extension "law" for the bridges. They applied the model to the propagation of full-scale cracks propagating under double cantilever loading and thereby demonstrated consistency with the measured T-curve response in a polycrystalline alumina.

Here we shall apply the Mai-Lawn bridging model to the mechanics of the indentation-strength test. It is appropriate to do this for two reasons. First, indentation cracks are strongly representative of the small "natural" flaws that control the strengths of ceramic materials in service.[1] Second, and most important, the indentation methodology will be seen to be ideally suited to quantitative analysis of the T-curve function. For this purpose, recourse will be made to several earlier sources of indentation-strength data, covering a broad spectrum of ceramic materials.[1,3,4,11] The consequent manner in which the indentation-strength test highlights one of the most important manifestations of T-curve behavior, namely flaw tolerance, will emerge as a uniquely appealing feature of the approach. The potential for using the attendant parametric evaluations in the T-curve analysis as a tool for investigating the role of chemical composition and processing variables as determinants of toughness properties is indicated.

2 Interfacial Crack Restraint Model

An earlier fracture mechanics model[10] for straight-fronted cracks restrained by interfacial bridging ligaments is reproduced here in modified form, appropriate to penny-like indentation cracks.

2.1 Equilibrium Crack Propagation

A fracture system is in equilibrium when the forces driving the crack extension are equal to the forces resisting this extension. Equilibria may be stable or unstable, depending on the crack-length dependence of these forces.[9] Here we shall characterize the driving forces by stress intensity factors $K(c)$, and the fracture resistance by toughness $T(c)$, where c is the crack size. We may consider separately the stress intensity factor arising from the applied loading, K_a, which is directly monitored, from that associated with any internal forces intrinsic to the microstructure, K_i, such as the ligamentary bridging forces we seek to include

here. We may then conveniently regard the fracture resistance of the material as the sum of an intrinsic interfacial toughness of the material T_0 and the internal K_i terms.[9] Hence our condition for equilibrium may be written

$$K_a(c) = T(c) = T_0 - \sum_i K_i(c) \qquad [1]$$

where we have summed over all internal contributions. We emphasize that T_0 is strictly independent of crack length. The quantity $T(c)$ is the effective toughness function, or T-curve, for the material. To obtain a rising T-curve, ie. an increase in toughness with crack length, the sum over the $K_i(c)$ terms must be either positive decreasing or negative increasing. In terms of Eq. 1 the condition for stability is that $dK_a/dc < dT/dc$ and for instability $dK_a/dc > dT/dc$.[9] We see then that a rising T-curve, where $dT/dc \geq 0$, will lead to increased stabilization of the crack system.

2.2 Microstructure-Associated Stress Intensity Factor

We seek now to incorporate the effect of restraining ligaments behind the growing crack tip into a microstructure-associated stress intensity factor, $K_a = \sum_i K_i$. In the context of indentation flaws we shall develop the analysis for cracks of half-penny geometry.

A schematic model of the proposed system is shown in Fig. 1. The interfacial bridging ligaments are represented as an array of force centers, $F(r)$, projected onto the crack pl Here c is the radius of the crack front and d is the characteristic separation of the centers. At very small crack sizes, $c < d$, the front encounters no impedance. As the front expands, bridges are activated in the region $d \leq r \leq c$. These bridges remain active until, at some critical crack size c^* ($>> d$), ligamentary rupture occurs at those sites most distant behind

the front. Thereafter a steady state annular zone of width $c^* - d$ simply expands outward with the growing crack.

The qualitative features of the crack response observed by Swanson et al[8] would appear to be well described by the above configuration. Enhanced crack stability arises from the increasing interfacial restraint as more and more bridging sites are activated by the expanding crack front (the number of active bridges will increase approximately quadratically with the crack radius). The discontinuous nature of the crack growth follows from the discreteness in the spatial distribution of the closure forces in the crack plane. Thus we imagine the crack to become trapped at first encounter with the barriers. If these barriers were to be sufficiently large the crack front could be "trapped " such that, at an increased level of applied stress, the next increment of advance would occur unstably to the second set of trapping sites. Further increases in applied stress would lead to repetitions of this trapping process over successive barriers, the jump frequency increasing as the expanding crack front encompasses more sites. There must accordingly be a smoothing out of the discreteness in the distribution of interfacial restraints as the crack grows until, at very large crack sizes, the distribution may be taken as continuous.

In principle, we should be able to write down an appropriate stress intensity factor for any given distribution of discrete restraining forces of the kind depicted in Fig. 1. However, an exact summation becomes intractable as the number of active restraining elements becomes large. To overcome this difficulty we approximate the summation over the discrete force elements, $F(r)$, by an integration over continuously distributed stresses, $\sigma(r) \simeq F(r)/d^2$. We plot these stresses for three crack configurations in Fig. 2. These stresses have zero value in the region $r < d$, reflecting the necessary absence of restraint prior to the intersection of the crack front with the first bridging sites. They have non-zero value in the region $d < r < c$ up to the crack size at which ligamentary rupture occurs ($d \leq c \leq c^*$), and thereafter in the

region $d + c - c^* < r < c$ where a steady state configuration is obtained ($c > c^*$). This approximation is tantamount to ignoring all but the first of the discontinuous jumps in the observed crack evolution. We might consider such a sacrifice of part of the physical reality to be justifiable in those cases where the critical crack configuration encompasses many bridging sites, as perhaps in a typical strength test.

The problem may now be formalized by writing down a microstructure-associated stress intensity factor in terms of the familiar Green's function solution for penny-like cracks [12]:

$$K_\mu = 0, \qquad (c < d) \qquad [2a]$$

$$K_\mu = -(\psi/c^{1/2}) \int_d^c \sigma(r)\, r\, dr/(c^2 - r^2)^{1/2}, \qquad (d \le c \le c^*) \qquad [2b]$$

$$K_\mu = -(\psi/c^{1/2}) \int_{d+c-c^*}^c \sigma(r)\, r\, dr/(c^2 - r^2)^{1/2}, \qquad (c > c^*) \qquad [2c]$$

where ψ is numerical crack geometry term. At this point another major difficulty becomes apparent. We have no basis, either theoretical or experimental, for specifying *a priori* what form the closure stress function $\sigma(r)$ must take. On the other hand, we do have some feeling from the observations of Swanson et al, albeit limited, as to the functional form $\sigma(u)$, where u is the crack opening displacement. Further, it is $\sigma(u)$ rather than $\sigma(r)$ which is the more fundamental bridging quantity, and which is more amenable to independent specification. Thus, given a knowledge of the crack profile, we should be able to replace r by u as the integration variable in Eq. 2 and thereby proceed one step closer to a solution.

However, even this step involves some uncertainty, as the crack profile itself is bound to be strongly influenced by the distribution of surface tractions; ie. $u(r)$ strictly depends on

$\sigma(r)$ (as well as on the applied loading configuration), which we have just acknowledged as an unknown. A rigorous treatment of this problem involves the solution of two coupled non-linear integral equations, for which no analytical solutions are available[13]. We thus introduce a simplification by neglecting any effect the tractions might have on the shape of the crack profile, while taking account of these tractions through their influence on the net driving force $K = K_e + K_\mu$ from Eq. 1, in determining the magnitude of the crack opening displacements. Accordingly, we choose Sneddon's solution[14] for the near-field displacements of an equilibrium crack, ie. $K = T_0$.

$$u(r,c) = (\psi T_0/Ec^{1/2})(c^2 - r^2)^{1/2} \qquad [3]$$

where E is the Young's modulus. Substitution of Eq. 3 into Eq. 2 then gives

$$K_\mu = 0, \qquad (c < d) \qquad [4a]$$

$$K_\mu = -(E/T_0)\int_0^{u(d,c)} \sigma(u)du, \qquad (d \le c \le c^*) \qquad [4b]$$

$$K_\mu = -(E/T_0)\int_0^{u^*} \sigma(u)du, \qquad (c > c^*) \qquad [4c]$$

We note that $u^* = u(d, c^*)$ is independent of c so K_μ cuts off at $c \ge c^*$.

Thus by sacrificing self-consistency in our solutions, we have obtained simple working equations for evaluating the microstructure-associated stress intensity factor. We have only to specify the stress-separation function, $\sigma(u)$.

2.3 Stress-Separation Function for Interfacial Bridges

The function $\sigma(u)$ is determined completely by the micromechanics of the ligamentary rupture process. We have indicated that we have limited information on what form this function should take. Generally, $\sigma(u)$ must rise from zero at $u = 0$ to some maximum and then decrease to zero again at some characteristic rupture separation u^*. The observations of crack propagation in alumina by Swanson et al suggest that it is the decreasing part of this stress-separation response which is the most dominant in the polycrystalline ceramics of interest here.[8] The stable crack propagation observed by those authors has much in common with the interface separation processes in concrete materials which are often described by tail-dominated stress-separation functions.

The stress-separation function chosen is[10]

$$\sigma(u) = \sigma^*(1 - u/u^*)^m \qquad (0 \le u \le u^*) \qquad [5]$$

where σ^* and u^* are limiting values of the stress and separation respectively and m is an exponent. We consider three values of m: $m = 0$ is the simplest case of a uniformly distributed stress acting over the annular activity zone; $m = 1$ corresponds to simple, constant-friction pullout of the interlocking ligamentary grains; $m = 2$ is the value adopted by the concrete community (equivalent to a decreasing frictional resistance with increasing pullout). As we shall see, the choice of m will not be too critical in our ability to describe observed strength data. Note that the representation of the stress-separation function by Eq. 5 is an infinite modulus approximation in that it totally neglects the rising part of the $\sigma(u)$ response.

Equation 5 may now be substituted into Eq. 4 to yield, after integration,

$$K_\mu = 0. \qquad (c < d) \qquad [6a]$$

$$K_\mu = -(T_\infty - T_0)\left\{1 - \left\{1 - \left[c^*(c^2 - d^2)/c(c^{*2} - d^2)\right]^{1/2}\right\}^{m+1}\right\} \qquad (d \le c \le c^*) \qquad [6b]$$

$$K_\mu = -(T_\infty - T_0), \qquad (c > c^*) \qquad [6c]$$

where we have eliminated the stress-separation parameters, σ^* and u^*, in favor of those characterizing steady-state crack propagation, c^* and T_∞:

$$c^* = 2(E\,u^*/\psi T_0)^2\left\{1 + \left[1 + 4(\psi T_0\, d^{1/2}/E\,u^*)^4\right]^{1/2}\right\} \qquad [7]$$

and

$$T_\infty = T_0 + E\,\sigma^*\,u^*/(m+1)T_0 \qquad [8]$$

These latter parameters are more easily incorporated into the strength analysis to follow.

A useful quantity is the work necessary to rupture an individual ligament. This work is a composite measure of the maximum sustainable stress and maximum range of the stress-extension function of Eq. 5 and is given by the area under the stress-separation curve, $\sigma(u)$. We may express this area as

$$\Gamma_\ell = \int_0^{u^*} \sigma(u)du = \sigma^*\,u^*/(m+1) \qquad [9a]$$

It is useful to compare this quantity with the intrinsic interfacial energy[9],

$$\Gamma_0 = T_0^2/2E \qquad [9b]$$

The Γ terms in Eq. 9 are related, through Eq. 8, by the ratio

$$\Gamma_i/\Gamma_0 = 2(T_\infty - T_0)/T_0 \qquad [10]$$

which may conveniently be regarded as a toughening index.

2.4 Strength-Indentation Load Relations

We are now in the position to consider the mechanics of a test specimen containing an indentation crack produced at load P and subsequently subjected to an applied stress σ_a. To obtain the "inert strength", σ_m, we need to determine the equilibrium instability configuration at which the crack grows without limit.

In indentation crack systems the stress intensity factor associated with the residual contact stresses, K_r, augments the stress intensity factor associated with the applied loading, K_a, effectively giving rise to a net applied stress intensity factor, K_a'. [15,16] Equation 1 becomes

$$\begin{aligned} K_a' &= K_a + K_r = T(c) \\ &= \psi\sigma_a c^{1/2} + \chi P/c^{3/2} = T_0 - K_\mu(c) \end{aligned} \qquad [11]$$

where χ measures the intensity of the residual field. We note that K_r is inverse in crack size and hence will further stabilize the fracture evolution.[16] The indentation load determines the initial crack size at $\sigma_a = 0$, but because of the stabilization in the growth we should not necessarily expect this initial size to be an important factor in the fracture mechanics. Our problem then is to combine Eqs. 6 and 11 and invoke the instability condition, $dK_a'/dc \geq dT/dc$, to determine the strength as a function of indentation load.

Unfortunately, it is not possible to obtain closed form solutions to this problem. Limiting solutions can be obtained analytically, however, and we consider these first:

(i) Small cracks (low P). In the region $c << d$ we revert to the ideal case of zero microstructural interaction, such that Eq. 6a applies. In this region it can be readily shown that the equilibrium function $\sigma_a(c)$ obtained by rearranging Eq. 11 passes through a maximum, up to which point the crack undergoes stable growth[16]. This maximum therefore defines the instability point $d\sigma_a/dc = 0$ (equivalent to the condition $dK_a'/dc = dT/dc = 0$ here);

$$\sigma_m^0 = 3T_0^{4/3}/4^{4/3}\psi(\chi P)^{1/3} \qquad [12]$$

The region of validity of this solution is indicated as Region I in Fig. 3.

(ii) Large cracks (high P). In the region $c >> c^*$ Eq. 6c applies and we have maximum microstructural interaction. The procedure to a solution is entirely the same as in the previous case, except that now T_∞ replaces T_0 in Eq. 12. Thus

$$\sigma_m^\infty = 3T_\infty^{4/3}/4^{4/3}\psi(\chi P)^{1/3} \qquad [13]$$

This solution applies in Region III in Fig. 3.

It is for intermediate cracks, Region II in Fig. 3, that analytical solutions are difficult to obtain. Here numerical procedures will be required, but the route is nevertheless the same as before; determine $\sigma_a(c)$ from Eq. 11 in conjunction with Eq. 6b and apply the instability condition, taking account of the increased stabilization arising from the K_a term. To proceed this way we must first determine the values of the parameters in Eqs. 6 and 11. We address this problem in the next section.

3 Derivation of T-curve from Indentation Strength Data

3.1 Crack Geometry and Elastic/Plastic Contact Parameters

Our first step towards a complete parametric evaluation of the $\sigma_m(P)$ data is to seek *a priori* specifications of the dimensionless quantities ψ and χ in Eq. 11. The parameter ψ is taken to be material-independent, since it is strictly a crack geometry term. The parameter χ does depend on material properties, however, relating as it does competing elastic and plastic processes in the indentation contact.[12] We note that these parameters do not appear in the microstructural term K_r in Eq. 6, so ideally we can we can "calibrate" them from tests on materials which do not exhibit T-curve behavior. The details of such calibrations are given in the Appendix. The values we use are $\psi = 1.24$ and $\chi = 0.0040(E/H)^{1/2}$, where H is the hardness.

3.2 Bounding Parameters for the Regression Procedure

We have indicated that solutions for Region II of the strength-load response of Fig. 3 must be obtained numerically. Here we shall outline the regression procedure used to deconvolute the T-curve for a given set of $\sigma_m(P)$ data.

To establish reasonable first approximations for a search/regression procedure, we note two experimental observations. The first is from the indentation/strength data of Cook et al[1]. In a number of materials the $\sigma_m(P)$ data tended strongly to the asymptotic limit of Region III at large indentation loads (Fig. 3), reflecting the upper, steady-state toughness T_∞ (see Eq. 13). No analogous transition corresponding to T_0 -controlled strengths in Region I was observed: at low indentation loads the strength data were truncated by failures from natural flaws. Notwithstanding this latter restriction, we may use Eqs. 12 and 13 (with "calibrated" values of ψ and χ from Sect. 3.1) to set upper bounds to T_0 and lower bounds to T_∞ from strength data at the extremes of the indentation load range. We expect from the observations

of Cook et al that the lower bound estimate of T_a probably lies closer to the true value than the upper bound estimate to T_0.

The second experimental observation is from the crack propagation work of Swanson et al,[8] who estimated the average distance bridging sites at two to five grain diameters. We accordingly take the lower bound estimate for the inter-ligament spacing d at one grain diameter. Similar bounding estimates for c^* are more difficult, although the condition $c^* > d$ must be satisfied.

There is one further parameter we have to specify, and that is the exponent of the ligament stress-extension function, m. We have alluded to the fact that the observations of Swanson et al indicate that a stabilizing, tail dominated stress-separation function should be appropriate, with $m \geq 1$ in Eq. 5.

3.3 Regression Procedure

With the first approximations thus determined we search for the set of parameters for each set of $\sigma_m(P)$ data. The scheme adopted to do this is as follows:

(1) The T-curve is set from Eqs. 1 and 6 and the equilibrium $\sigma_a(c)$ response is calculated from Eq. 11 at each indentation load for which there are measured strength data.

(2) The predicted strength at each indentation load is determined numerically from the instability requirement $d\sigma_a/dc = 0$ (with the proviso that if more than one maximum in the $\sigma_a(c)$ function exists, it is the greater which determines the strength - see Sect. 4).

(3) The predicted strengths are compared with the corresponding measured strengths and the mean variance thereby calculated for a given set of T-curve parameters.

(4) The T-curve parameters are incremented and the calculation of the variance repeated, using a matrix search routine. The increments in the search variables were 0.05 MPa $m^{1/2}$ for the toughness parameters T_0 and T_∞ and 5 μm for the dimension parameters d and c^*.

(5) The set of T-curve parameters yielding the minimum residual variance is selected.

4 Results

The materials analyzed in this study are listed in Table I, along with their Young's modulus, hardness, grain size and minor phase percentage. Previously published [1,3,4,11] indentation-strength data for these materials * was used for the T-curve deconvolutions. The resultant parameter evaluations are given in Table II.

Our first exercise was to select a fixed value of the exponent m for the T-curve evaluations. Accordingly a preliminary analysis of the $\sigma_\infty(P)$ data for two materials displaying particularly strong T-curve influences in their strength responses, namely the VI1 and VI2 aluminas, was carried out. Figure 4 shows the minimum residual mean deviation as a function of m for these materials. The deviation for both materials is greatest at $m = 0$ but thereafter at $m \geq 1$ is insensitive to the choice of exponent. The value somewhat arbitrarily chosen for this study was $m = 2$ in accord with that adopted in the concrete literature.[10]

To illustrate the procedure and at the same time to gain valuable insight into the crack evolution to failure let us focus now on just two of the listed alumina materials in Table I, VI2 and AD96. Figure 5 shows the strength vs indentation load data for these materials.[1] The data points in this figure represent means and standard deviations of approximately ten strength tests at each indentation load. The solid lines are the best-fits (Eqs. 1, 6 and 11) to

---

* Some data were removed from the original $\sigma_\infty(P)$ data sets at large indentation loads, where the influence of secondary lateral cracking was suspected to have significantly decreased the magnitude of the residual stress intensity factor [17].

the data. The dashed lines represent T_0 - and T_∞-controlled limits (Eqs. 12 and 13). As can be seen the fitted curves smoothly intersect the T_∞-controlled limit at large indentation loads, this tendency being greater for the AD96 material. This smooth connection is a reflection of our choice of m above; for $m < 2$ the $\sigma_m(P)$ curve intersects the T_∞ limit with a discontinuity in slope. At intermediate indentation loads the strengths tend to a plateau level, more strongly for the VI2 material. In line with our contention that this plateau is associated with a strong microstructural influence we might thus expect the VI2 material to exhibit a more pronounced T-curve. The larger separation of the T_0- and T_∞-controlled limits for the VI2 material in Fig. 6 supports this contention. Finally at small indentation loads the strengths cut off abruptly at the T_0-controlled limit, corresponding to the case where the crack intersects no bridges prior to unlimited instability.

Figures 6 and 7 show the corresponding equilibrium $\sigma_a(c)$ and $T(c)$ functions which underlie the curve fits in Fig. 5. The $\sigma_a(c)$ responses are plotted for several indentation loads, embracing the data range covered in the indentation-strength experiments (eg. Fig. 5). The most distinctive feature of these curves is that at low indentation loads, where the initial crack size is somewhat smaller than the first barrier distance d, there are two maxima, most notably in the VI2 material. The first maximum, at $c < d$ is a pure manifestation of the crack stabilization due to the residual contact stress term (Eq. 11).[16] The second maximum, at $c > d$, results from the additional, abrupt stabilization associated with the microstructural closure forces. Of the two maxima, it is the greater which determines the strength. Thus at very low P (corresponding to Region I in Fig. 3) the first maximum wins, and the instability takes the crack system to failure without limit (eg. the $P = 0.1$ N curves for both the VI2 material in Fig. 6 and the AD96 material in Fig. 7). At intermediate P (Region II in Fig. 3) the second maximum becomes dominant, in which case the crack arrests before failure can ensue (eg. the $P = 1$N curves in Figs. 6 and 7). Note that the second maximum for the VI2

alumina occurs at ≈ 100 μm, consistent with abrupt initial jumps of 2-5 grain diameters reported by Swanson et al. At large P (Region III in Fig. 3) the curves tend more and more to a single pronounced maximum, as we once more enter a region of invariant toughness.

It is in the transition region, Region II, where the form of the T-curve most strongly influences the crack stability and strength properties. The T-curve for the VI2 alumina rises more steeply than that for the AD96 alumina. The difference in responses for the two materials may be seen most clearly in the $\sigma_a(c)$ curves for P = 10 N, Figs. 6 and 7. In VI2 alumina the restraint exerted on the crack by the interfacial bridges is apparently much stronger than in AD96. We note that the indentation-strength curves in Fig. 5 may be seen as "rotated" versions of the T-curves in Figs. 6 and 7.

A word is in order here concerning the "sensitivity" of the parameter evaluations to the range of data. Figure 8 shows the deconvoluted T-curves for the VI2 material with individual data points at either end of the indentation load range deliberately omitted from the base data in Fig. 5a. When data are "lost" from the large P end the high $T(c)$ part of the curve is most affected; similarly for data omissions at the small P end the low $T(c)$ part of the curve is most affected. We may regard the curve shifts in Fig. 8 as characterizing the systematic uncertainty in our parameter evaluations, just as the mean residual deviation in the regression procedure characterizes the random uncertainty. We note that it is those parameters which control the upper and lower bounds of the T-curve which are subject to the greatest uncertainty, since it is in these extreme regions (especially in the T_0 -controlled region) where indentation-strength data are most lacking. The central portions of the T-curves in Fig. 8 are not altered substantially by the deletion of strength data.

Subject to the above considerations, we may now usefully summarize the relative T-curve behavior for the remainder of the materials listed in Table II. The T-curves are shown in Figs. 9 to 11 for each of the material types, aluminas, glass-ceramics and barium titanates.

Special attention may be drawn to the fact that the curves for the microstructurally variant materials in each of these composite plots tend to cross each other. We note in particular that the curves for the polycrystalline aluminas in Fig. 9 cross below that for sapphire at small crack sizes, consistent with earlier conclusions that the intrinsic polycrystal toughness (T_0) is governed by grain boundary properties.[1]

5 Discussion

We have considered a fracture toughness model based on an independently verified interface restraint mechanism [8,9] for explaining the microstructural effects previously reported in indentation/strength data.[1-4] A key feature of our modelling is the strong stabilizing effect of grain-scale ligamentary bridges on the stability conditions for failure. * Although the earlier experimental observations used to establish the model[8] were based almost exclusively on one particular alumina ceramic[1] our own detailed crack observations, and those of others, strongly suggest that the model is generally applicable to other non-transforming ceramics; the discontinuous primary crack traces characteristic of the bridging process have since been observed in other aluminas, [18,19] glass-ceramics, [18-20] SiC ceramics,[21] and polymer cements.[19] The fact that the resultant strength equations from the model can be fitted equally well to all the materials examined in the present study serves to enhance this conviction.

A characteristic feature of the failure properties of the materials with pronounced T-curves (eg. VI2 alumina) is the relative insensitivity of the strength to initial flaw size. This is a vital point in relation to structural design. Materials with strong T-curve responses have

---

* In this sense our explanation differs somewhat from that originally offered by us in Ref. 1, where it was tacitly suggested that the microstructural influence might be represented as a positive decreasing function of crack size. The distinction between negative increasing and positive decreasing K_r functions is not easily made from strength data alone.

the quality of flaw tolerance. Ideally, it would seem that one should seek to optimize this quality. Associated with this tolerance is an enhanced crack stability. This offers the potential detection of failures. On the other hand, there is the indication that such benefits may only be wrought by sacrificing high strengths at small flaw sizes. This tendency is clearly observed in the way the strength curves cross each other in Figs. 7 to 9 in Ref. 1 (corresponding to crossovers seen here in the T-curves, Figs. 9 to 11). In other words the designer may have to practise the gentle art of compromise.

We reemphasize that the T-curve parameters derived from the strength data (Table II) are elements of curve-fitting and are subject to systematic as well as to the usual random uncertainties. Since any four of these parameters are independent our numerical procedure, regardless of "goodness of fit", cannot be construed as "proof" of our model. Nevertheless, we may attach strong physical significance to these parameters. For example, the relatively large values of Γ_f and c^* for the VI materials relative to the corresponding parameters for the F99 alumina is a clear measure of a greater T-curve effect in the former. More generally, the aluminas with glassy phases at their grain boundaries,[22] or with smaller grain size (Tables I and II) have relatively low toughness indices, Γ_f/Γ_0, indicating that there is some kind of trade-off between macroscopic and microscopic toughness levels, and that this trade-off is controlled by the microstructure. We note also that the maximum stress-separation range parameters u^* for the materials are in the range 0.1 - 0.4 μm, consistent with crack opening displacement observations at the bridging sites.[6,18-21] We thus suggest that such parameters could serve as useful guides to materials processors, for tailoring materials with desirable, pre-determined properties, especially with regard to grain boundary structure.

Mention was made in Sect. 4 of the sensitivity of the parameter evaluations to the available data range. This has implications concerning conventional, large-crack toughness measurements. To investigate this point further we plot in Fig. 12 the T_s values determined here

against those measured independently by macroscopic techniques. The degree of correlation in this plot would appear to lend some confidence to our fitting procedure (and to our *a priori* choices for the parameters ψ and χ). Since most of our strength data tend to come from regions towards the top of the T-curve we should perhaps not be too surprised at this correlation.

Finally, we may briefly address the issue of test specimen geometry in connection with the accuracy of the parameter evaluations. It has been argued elsewhere[9] that test specimen geometry can be a crucial factor in the T-curve determination. It might be argued for instance that "superior" parameter evaluations could be obtained from larger crack geometries, particularly the c^*, T_* parameters. However, the indentation methodology takes us closer to the strengths of specimens with natural flaws, in particular to the T_0-controlled regions (notwithstanding our qualifying statements earlier concerning this parameter), so that the present evaluations may be more appropriate for designers.

6 Conclusions

1. An independently confirmed ligament bridging model is used as the basis for analyzing observed indentation-strength data for a wide range of polycrystalline ceramic materials.

2. Those materials with pronounced T-curves show the qualities of "flaw tolerance" and enhanced crack stability.

3. A fracture mechanics treatment of the indentation fracture system with microstructure-associated factors incorporated allows for the (numerical) deconvolution of toughness/crack-length (T-curve) functions from these data.

4. Comparisons within a range of aluminas suggests that those materials with "glassy" grain boundaries and smaller grain size have less pronounced T-curves than those with "clean" boundaries.

5. The indentation-strength technique and the toughness parameters deriving from it should serve as useful tools for the development of ceramic materials with predetermined properties, especially with respect to grain boundary structure and chemistry.

Appendix - Evaluation of ψ and χ

Here we derive numerical values for the dimensionless parameters ψ and χ characterizing the crack geometry and the intensity of the residual contact stress, respectively. The choices for these should yield agreement between measured strength and toughness properties of homogeneous materials with no measurable T-curve behavior (ie. $K_s = 0$, $T = T_0 = T_s$).

We begin with the geometrical ψ term, which is assumed to be material independent. From the applied stress (strength) σ_m and crack length c_m at the instability point of an indentation we can show that[23]

$$\psi = 3T/4(\sigma_m c_m^{1/2}) \qquad [A1]$$

Measurements of $\sigma_m c_m^{1/2}$ for several homogeneous materials confirm that Eq. A1 describes the toughness/instability properties,[23,24] for $\psi = 1.24$. We note that this is very close to the value of 1.27 calculated by finite element analyses of semi-circular cracks in surfaces of bend specimens.[25]

For the χ term we turn to Ref. 12, where it is shown that

$$\chi = \xi(E/H)^{1/2} \qquad [A2]$$

where ξ is a material independent constant. With this result Eq. 12 may be re-written as[26]

$$T_0 = \eta(E/H)^{1/8}(\sigma_m^0 P^{1/3})^{3/4} \qquad [A3]$$

where

$$\eta = (256\psi^{1/3}\xi/27)^{1/4} \qquad [A4]$$

is another material-independent constant. From measurements of $\sigma_m^0 P^{1/3}$ for a similar range of homogeneous materials we obtain $\eta = 0.52$.[24] Hence, eliminating ξ from Eqs. A2 and A4 yields

$$\chi = 27\eta^4 (E/H)^{1/2}/256\psi^3 \qquad [A5]$$

which gives $\chi = 0.0040(E/H)^{1/2}$.

Acknowledgements

The authors thank C. Thompson for assistance with some of the computer programs used in this work. Funding for the NBS component of this work was provided by the US Army Research Office.

Tables

Table I - Materials Analyzed in this Study

Material		Young's Modulus E/GPa	Hardness H/GPa	Grain Size μm	Minor Phase %	Ref.
Alumina	VI1	393	19.1	20	0.1	1
	VI2	393	19.0	41	0.1	1
	AD999	386	20.1	3	0.1	1
	AD96	303	14.1	11	4	-
	AD90	276	13.0	4	10	1
	F99	400	16.1	11	1	1
	HW	206	11.7	28	0.3	1
	Sapphire	425	21.8	-	-	1
Glass-Ceramics	SL1	87.9	4.4	1.2	33	1.3
	SL2	87.9	4.3	1.9	22	1.3
	SL3	87.9	4.8	2.3	20	1.3
	Macor	64.1	2.0	17	50	4
	Pyroceram	108	8.4	1	-	4
Barium Titanate	CH(cub.)	123	5.9	7	1	11
	CH(tet.)	123	5.9	7	1	11

Table II - T-curve Parameters Derived from Strength Data (From Refs. 1, 3, 4, 11)

Material	T_0 (MPa m$^{1/2}$)	T_∞ (MPa m$^{1/2}$)	Γ_0 (J m^{-2})	Γ_f (J m^{-2})	d (μm)	c^* (μm)	σ^* (MPa)	u^* (μm)
VI1	1.73	4.08	3.8	10.4	40	420	280	0.11
VI2	1.49	4.63	2.8	11.8	60	540	328	0.11
AD999	2.22	4.30	6.4	12.0	15	715	188	0.19
AD96	2.16	2.87	8.5	5.6	15	460	80	0.19
AD90	2.76	3.21	13.8	4.6	15	210	75	0.18
F99	2.70	3.50	9.1	5.4	15	30	405	0.04
HW	2.64	4.31	16.9	21.4	95	710	153	0.42
Sapphire	3.10	3.10	11.3	0	-	-	-	-
SL1	1.06	1.98	6.4	11.2	10	335	122	0.27
SL2	1.12	2.29	7.1	15.0	10	485	129	0.35
SL3	1.35	2.58	10.4	19.0	25	505	133	0.43
Macor	1.04	2.30	8.4	20.4	40	535	132	0.46
Pyroceram	2.04	2.33	19.3	5.4	20	415	35	0.48
CH(c)	0.95	0.95	3.7	0	-	-	-	-
CH(t)	0.79	1.35	2.5	3.6	40	330	70	0.14

References

[1]R.F. Cook, B.R. Lawn and C.J Fairbanks, J.Am.Ceram.Soc. **68**, 604 (1985)

[2]R.F. Cook, B.R. Lawn and C.J Fairbanks, J.Am.Ceram.Soc. **68**, 616 (1985)

[3]R.F. Cook, S.W. Freiman and T.L. Baker, Mat.Sci.Eng. **77** , 199 (1986)

[4]C.J. Fairbanks, B.R. Lawn, R.F. Cook and Y-W Mai, in *Fracture Mechanics of Ceramics*, Vol. 8, edited by R.C. Bradt, A.G. Evans, D.P.H. Hasselman and F.F. Lange (Plenum, New York, 1986) pp. 23-37.

[5]H. Hübner and W. Jillek, J.Mater.Sci. **12** , 117 (1977)

[6]R. Knehans and R. Steinbrech, J.Mater.Sci.Letters **1** , 327 (1982)

[7]R. Steinbrech, R. Knehans and W. Schaawächter, J.Mater.Sci. **18** , 265 (1983)

[8]P.L. Swanson, C.J. Fairbanks, B.R. Lawn, Y-W Mai and B.R. Hockey, J.Am.Ceram.Soc., in press

[9]Y-W Mai and B.R. Lawn, Ann.Rev.Mater.Sci. **16** , 415 (1986)

[10]Y-W Mai and B.R. Lawn, J.Am.Ceram.Soc., in press

[11]R.F. Cook, S.W. Freiman, B.R. Lawn and R.C. Pohanka, Ferroelectrics **50** , 267 (1983)

[12]B.R. Lawn, A.G. Evans and D.B. Marshall, J.Am.Ceram.Soc. **63** , 574 (1980)

[13]D.R. Clarke, B.R. Lawn and D.H. Roach, in *Fracture Mechanics of Ceramics*, Vol. 8, edited by R.C. Bradt, A.G. Evans, D.P.H. Hasselman and F.F. Lange (Plenum, New York, 1986) pp. 341-350

[14]I.N. Sneddon, Proc.Roy.Soc.Lond. **A187** , 229 (1946)

[15]D.B. Marshall and B.R. Lawn, J.Mater.Sci. **14** , 2001 (1979)

[16]D.B. Marshall, B.R. Lawn and P. Chantikul, J.Mater.Sci. **14** , 2225 (1979)

[17]R.F. Cook and D.H. Roach, J.Mater.Res. **1** , 589 (1986)

[18]P.L Swanson, to be published in *Advances in Ceramics*, (American Ceramic Society, Inc.)

[19]R.F. Cook, unpublished work

[20]K.T. Faber and A.G. Evans, Acta Metall. **31** , 577 (1983)

[21]K.T. Faber and A.G. Evans, J.Am.Ceram.Soc. **66** , C-94 (1983)

[22]S.L. Fortner, unpublished work

[23]R.F. Cook and B.R. Lawn, J.Am.Ceram.Soc. **66** , C-200 (1983)

[24]R.F. Cook, Ph.D. Thesis, University of New South Wales, Australia. (1985)

[25]J.C. Newman and I.S. Raju, Eng.Frac.Mech. **15**, 185 (1981)

[26]P. Chantikul, G. Anstis, B.R. Lawn and D.B. Marshall, J.Am.Ceram.Soc. **64**, 539 (1981)

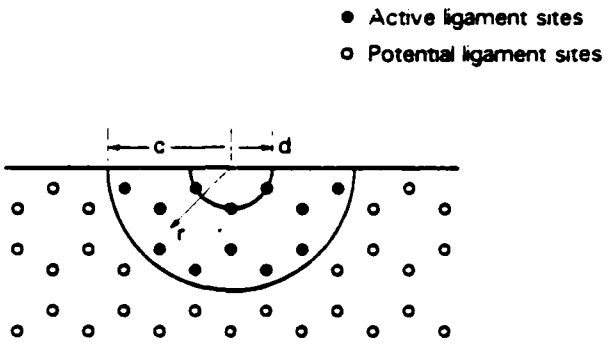

Figure 1. Schematic diagram of a half-penny, surface crack propagating through a material with bridging ligaments impeding the crack motion. Here d is the mean ligament spacing, c is the crack radius, and r is the radial coordinate from the penny origin.

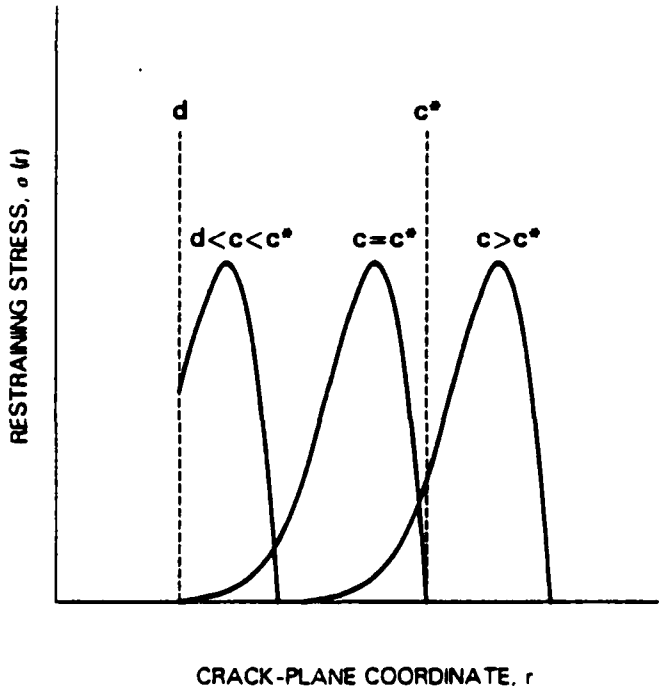

Figure 2. Stress distribution applied by the restraining ligaments over the crack plane as a function of radial distance from the center of the crack. Note that the stress is zero for $r < d$ and reaches a steady state distribution for $c \geq c^*$.

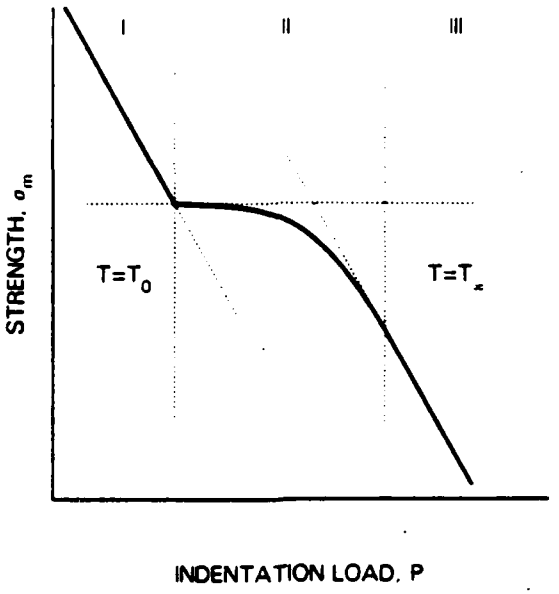

Figure 3. Schematic strength vs indentation load plot incorporating the influence of bridging ligaments into the crack propagation response (logarithmic coordinates). The solid line represents the general solution (Eqs. 6 and 11). The dashed lines represent asymptotic solutions obtained analytically for small cracks (Region I, Eq. 12) and large cracks (Region III, Eq. 13).

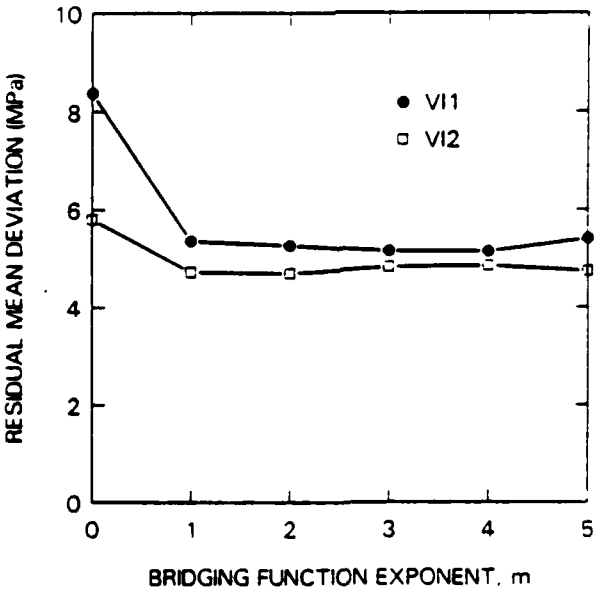

Figure 4. The residual mean deviation between fitted and measured indentation-strength functions vs bridging function exponent m for the VI aluminas. Note the relative insensitivity for $m \geq 1$.

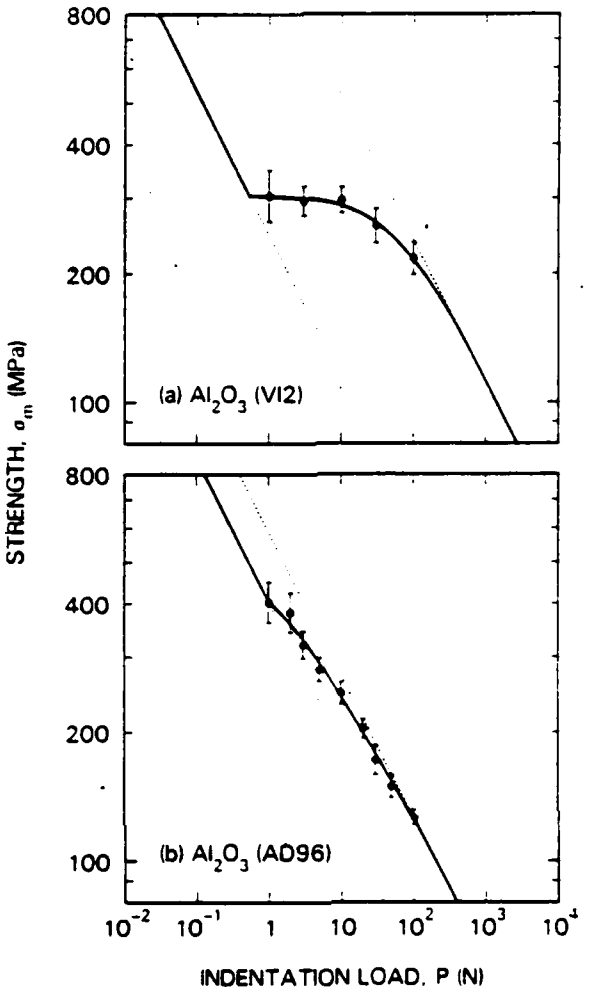

Figure 5. Indentation-strength data fits for the VI2 and AD96 aluminas. Note the relatively pronounced plateau for the VI2 material, indicative of a strong T-curve influence. Oblique dashed lines are T_0- and T_s-controlled limiting solutions.

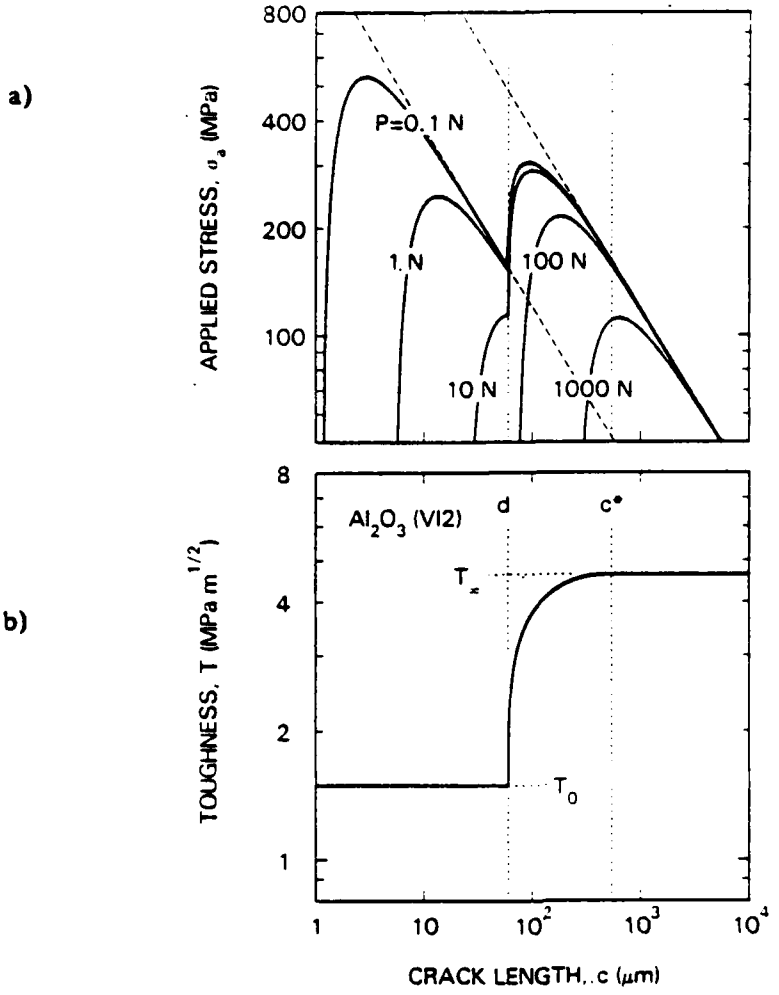

Figure 6. (a) Applied stress vs equilibrium crack length at different indentation loads, and (b) corresponding T-curve, for VI2 alumina, as derived from the indentation-strength data in Fig. 5.

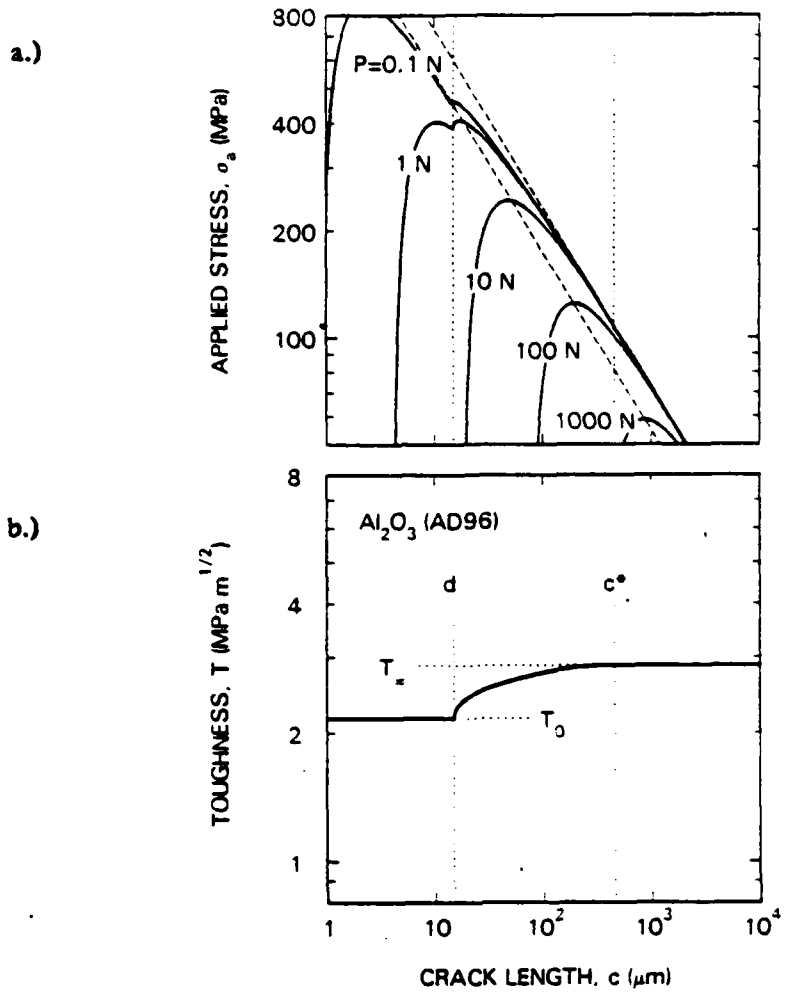

Figure 7. (a) Applied stress vs equilibrium crack length, and (b) corresponding T-curve, for AD96 alumina.

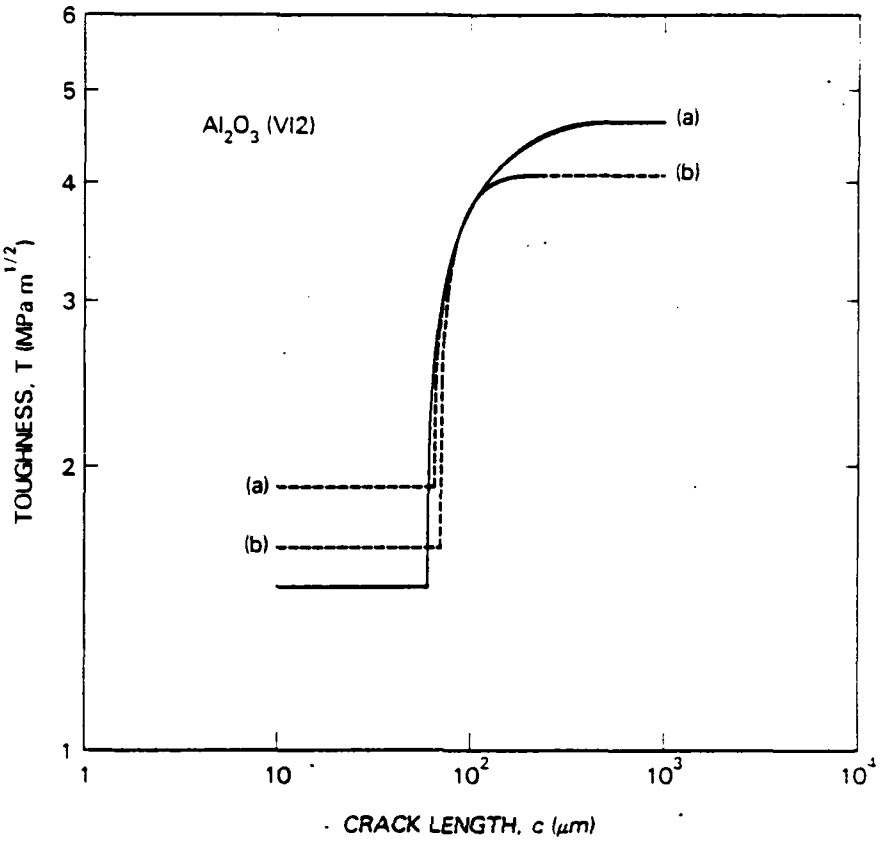

Figure 8. Deconvoluted T-curve plots for the VI2 alumina using full indentation-strength data set from Fig. 5a (solid line) and same data truncated (dashed lines) by removal of extreme data points at (a) low P and (b) high P.

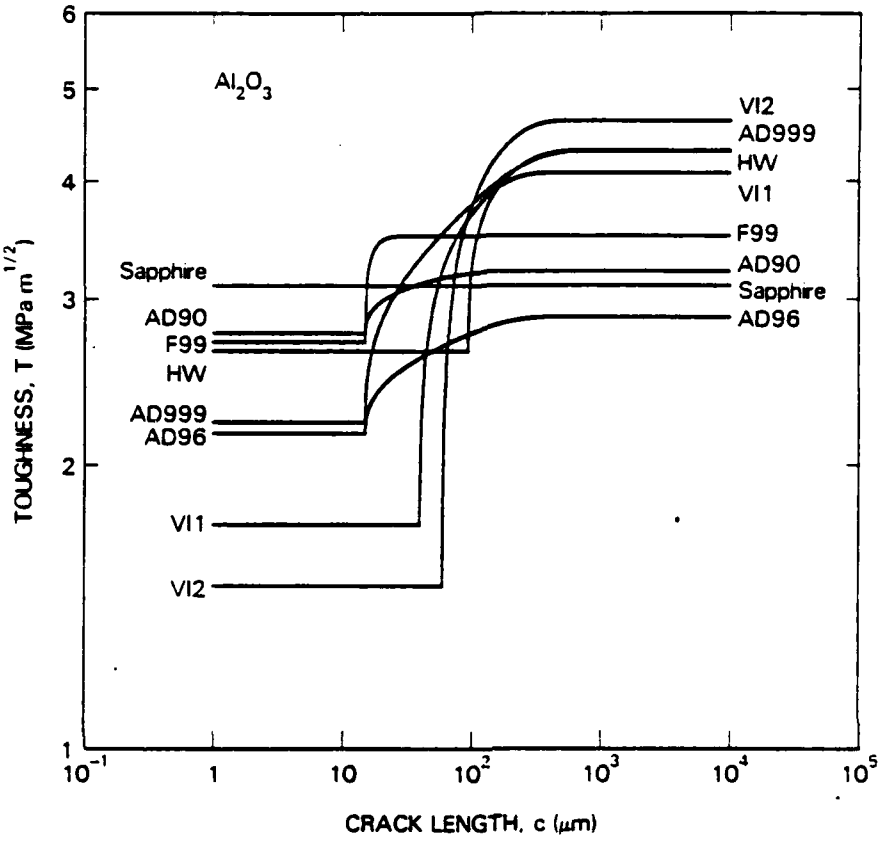

Figure 9. Composite plot of the deconvoluted T-curves for the alumina materials.

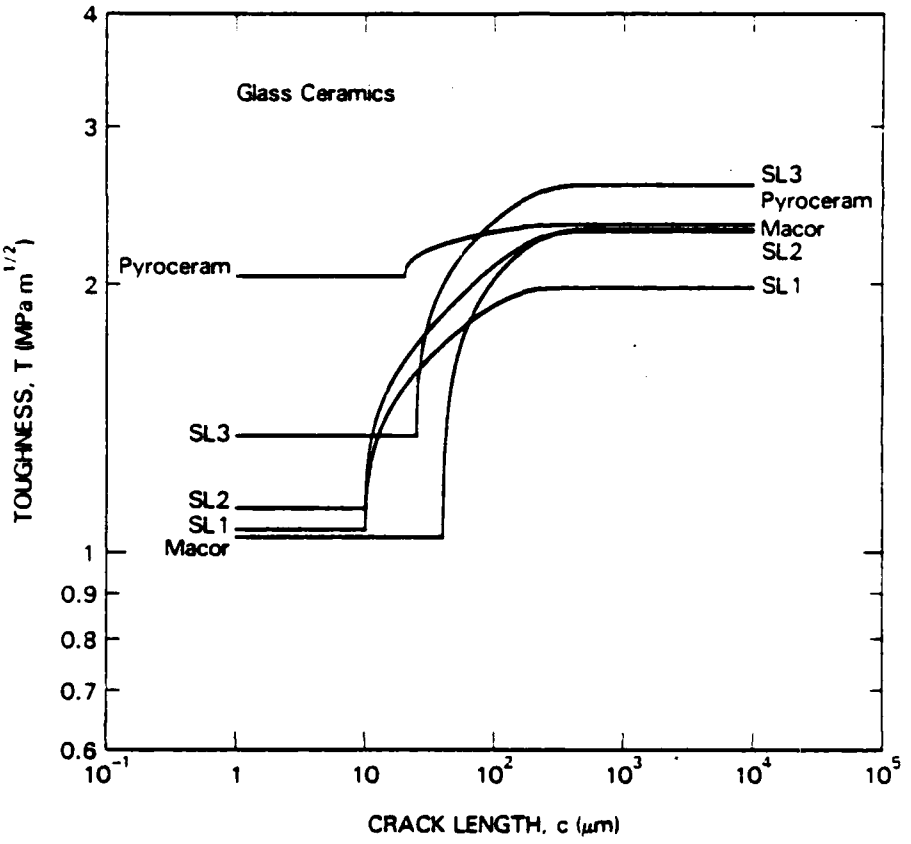

Figure 10. Composite plot of the deconvoluted T-curves for the glass-ceramic materials.

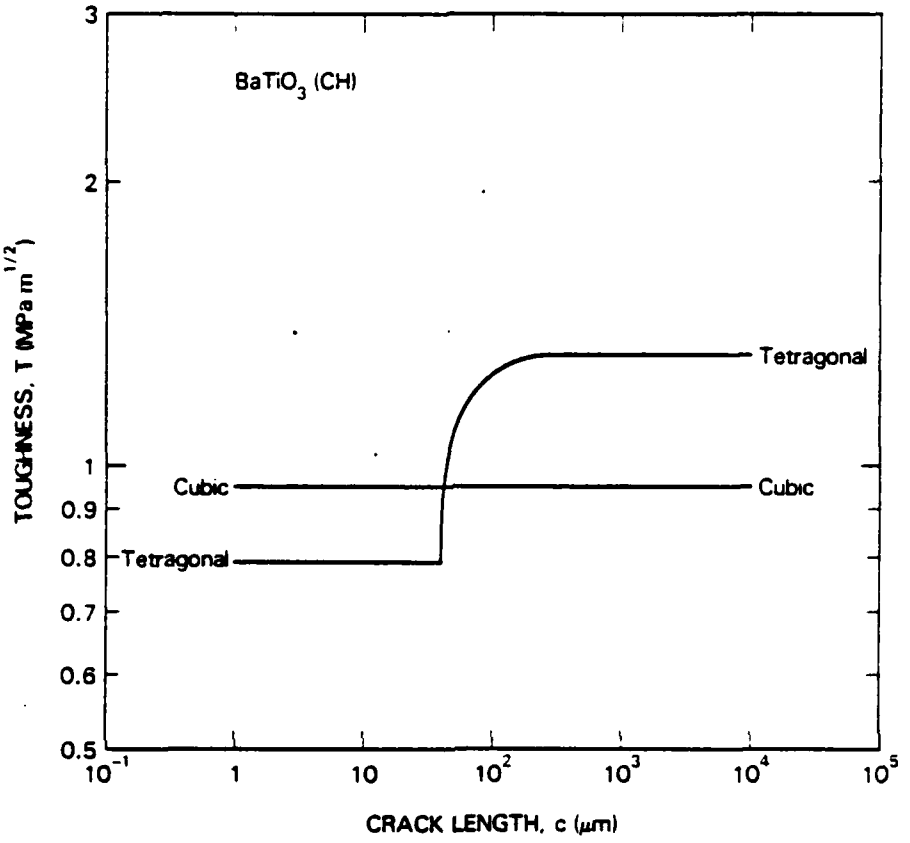

Figure 11. Composite plot of the deconvoluted T-curves for the barium-titanate material.

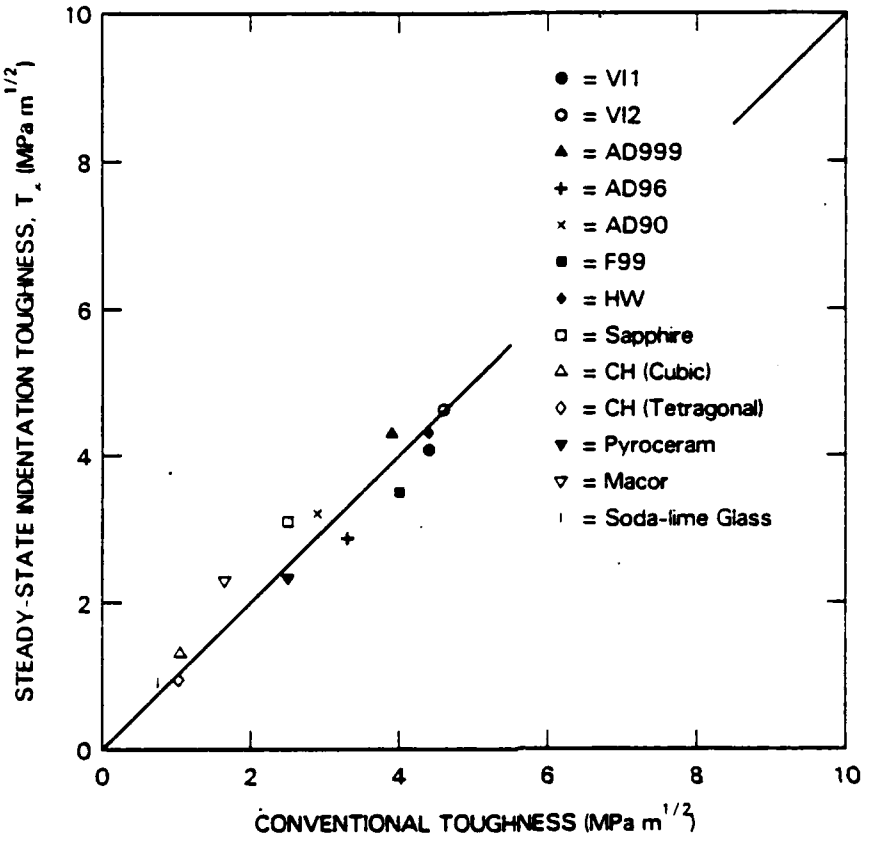

Figure 12. Plot of T_s (Table II) as a function of independently measured toughness using conventional macroscopic specimens.

MICROSTRUCTURAL EFFECTS ON GRINDING OF ALUMINA AND GLASS CERAMICS

David B. Marshall
Rockwell International Science Center
1049 Camino Dos Rios
Thousand Oaks, CA 91360

Brian R. Lawn
Ceramics Division
National Bureau of Standards
Gaithersburg, MD 20899

Robert F. Cook
I.B.M.
Thomas J. Watson Research Center
Yorktown Heights, NY 10598

ABSTRACT

Grinding forces were measured in aluminas and glass-ceramics with various microstructures. The microstructures were found to exert a profound influence on the machinability. In particular, the controlling toughness variable is that which pertains to small cracks, not that conventionally measured in a large-scale fracture specimen.

It is well documented that the principal material variable in microfracture-controlled properties of brittle ceramics, such as erosion, wear and machining, is the "toughness".[1] This is in accord with intuition: the greater the resistance to fracture, the harder it should be to remove material in localized, cumulative, surface contact processes. Implicit in existing material removal theories is the presumption that toughness is a single-valued quantity for a given material. Recent studies of the fracture properties of a wide range of ceramics call this presumption into serious question; toughness is generally <u>not</u> a material constant, but rather some increasing function of crack size (R-curve, or T-curve).[2] In certain aluminas, for example, the toughness can increase by a factor of three or so, depending on the microstructure.[3,4] The T-curve effect is seen most strongly in those aluminas with larger grain sizes and lower content of grain boundary glassy phase. Most interestingly, the T-curves for different aluminas tend to cross each other,[4] so that the toughness rankings at large and small crack sizes appear to be reversed. Clearly, if we wish to retain toughness as an indicator of wear resistance we need to qualify the scale on which this parameter is determined.

Accordingly, surface grinding tests were made on selected ceramic materials for which well-characterized T-curve data are available. The primary materials were aluminas from a previous study,[4] where the resistance characteristics were determined from the strengths of specimens containing indentation flaws. In addition, two commercial glass-ceramics were tested. A subsequent quantitative analysis of the indentation-strength data has

---

Only those materials originally available in disk form in that earlier work were selected. The strength data for these specimens are not limited by edge failures, so the resistance characteristics are more likely to refect the intrinsic microstructural influence.[4]

provided upper (large crack size) and lower (small crack size) bounds, T_∞ and T_o, to the T-curves for these materials.[5] Table 1 lists these parameters for comparison with the grinding results.

The grinding forces were measured using a dynamometer on the table of a diamond wheel (240 grit, width 10 mm) surface grinding machine. Runs were made at fixed depths of cut, 5, 10, 15, 20 μm, wheel rotation speed 3300 r.p.m. and horizontal feed rate 16 $mm \cdot s^{-1}$, with water-soluble oil lubrication. The specimens were first cut into bars of width 5 mm and then mounted in a row on the dynamometer so that force measurements could be made on all materials in a single pass at fixed depth of cut. The results are plotted in Fig. 1. It will be noted from the relative positions of the curves that the aluminas and glass-ceramics have been ranked in order of diminishing grinding resistance in Table 1.

It is immediately apparent from Fig. 1 that different aluminas and different glass-ceramics can vary widely in their grinding resistance. Thus the alumina with the highest resistance in Table 1 (i.e. AD90) is that with the greatest glassy content. This may come as no surprise to those who prepare ceramic powders by ball milling: alumina spheres with high glass content are found to be far more durable than similar spheres of high purity.[6] It may also be noted from Table 1 that for aluminas of comparable purity those with higher grinding resistance have finer grain sizes (cf. A999 and Vistal). Most interesting, however, is the quantitative correlation between grinding resistance and toughness parameters. The macroscopic toughness T_∞ (i.e. the toughness K_{IC} we measure in conventional large-scale fracture tests) actually shows an <u>inverse</u> correlation with the grinding resistance. On the other hand, the microscopic toughness T_o does appear to scale in the right direction. The data for the two glass-ceramics in Table 1

serve to reinforce the point; on the basis of the T_∞ values we would be unable to choose between the two materials, whereas the relative values of T_o confirm "Macor" (specified as a "machinable" glass-ceramic by its manufacturer) as the material of lower grinding resistance.

We conclude, therefore, that the time-honored conception of "toughness" as a universal indicator of superior mechanical properties, at least on the microscale, needs to be carefully qualified. The use of conventional fracture toughness evaluations to predict resistance to wear, erosion, and machining may lead to imprudent choices of materials for structural applications. On the positive side, a more complete understanding of the micromechanics that determine the complete crack resistance curve may ultimately help us optimize microstructural elements (glass content, grain size, etc.) for minimum surface degradation.

ACKNOWLEDGEMENTS

Funding provided by Rockwell Independent Research and Development Program (DBM) and the U.S. Army Research Office (BRL).

REFERENCES

1. A.W. Ruff and S.M. Wiederhorn: Ch. 2 in "Materials Erosion," Treatise on Materials Science and Technology, Vol. 16. Edited by C.M. Preece. Academic, New York, 1979.

2. Y-W. Mai and B.R. Lawn, Crack Stability and Toughness Characteristics in Brittle Materials," Ann. Rev. Mater. Sci. 16, 415-39 (1986).

3. R. Knehans and R. Steinbrech, "Memory Effects of Crack Resistance During Slow Crack Growth in Notched Alumina Specimens," J. Mater. Sci. Lett. 1[8] 327-29 (1982).

4. R.F. Cook, B.R. Lawn, and C.J. Fairbanks, "Microstructure-Strength Properties in Ceramics: I," J. Am. Ceram. Soc. 68[11] 604-15 (1985).

5. R.F. Cook, C.J. Fairbanks, B.R. Lawn, and Y-W. Mai, J. Mater. Research, to be published.

6. F.F. Lange; private communication.

Table 1. Comparison of toughness and grinding resistance parameters for the materials used in this study. T_∞ and T_o evaluated from indentation-strength data (Ref. 5). Material rankings in order of decreasing resistance (from Fig. 1).

Material			Additive (%)	Grain size (μm)	T_∞ (MPa·m$^{1/2}$)	T_o (MPa·m$^{1/2}$)
Alumina	AD90	a	10	4	3.2	2.8
	Sapphire	b	-	-	3.1	3.1
	AD96	a	4	11	2.9	2.2
	AD999	a	0.1	3	4.3	2.2
	Vistal I	a	0.1	20	4.1	1.7
	Vistal II	a	0.1	40	4.6	1.5
Glass-ceramic	Pyroceram	c	-	1.5	2.3	2.0
	Macor	c	-	13	2.3	1.0

a. Coors Porcelain Co., Golden, CO

b. Adolf Meller Co., Providence, RI

c. Corning Glass Co., Corning, NY

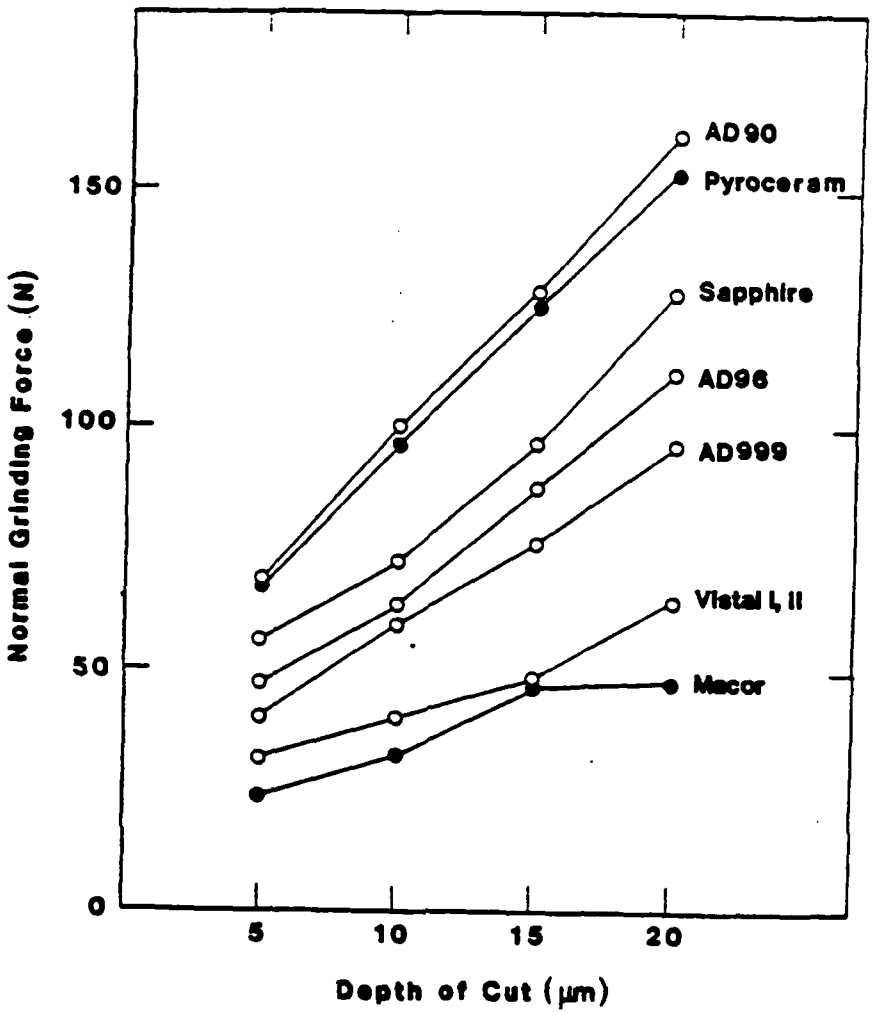

Fig. 1. Vertical grinding forces as function of depth of cut. Open symbols, aluminas; closed symbols, glass ceramics.

UNCLASSIFIED
SECURITY CLASSIFICATION OF THIS PAGE

REPORT DOCUMENTATION PAGE

1a. REPORT SECURITY CLASSIFICATION Unclassified	1b. RESTRICTIVE MARKINGS
2a. SECURITY CLASSIFICATION AUTHORITY	3. DISTRIBUTION/AVAILABILITY OF REPORT Approved for public release; distribution unlimited.
2b. DECLASSIFICATION/DOWNGRADING SCHEDULE	
4. PERFORMING ORGANIZATION REPORT NUMBER(S)	5. MONITORING ORGANIZATION REPORT NUMBER(S) ARO 21521.3-MS
6a. NAME OF PERFORMING ORGANIZATION National Bureau of Standards 6b. OFFICE SYMBOL (If applicable)	7a. NAME OF MONITORING ORGANIZATION U. S. Army Research Office
6c. ADDRESS (City, State, and ZIP Code) Bldg. 223, Room A335 Gaithersburg, MD 20899	7b. ADDRESS (City, State, and ZIP Code) P. O. Box 12211 Research Triangle Park, NC 27709-2211
8a. NAME OF FUNDING/SPONSORING ORGANIZATION U. S. Army Research Office 8b. OFFICE SYMBOL (If applicable)	9. PROCUREMENT INSTRUMENT IDENTIFICATION NUMBER
8c. ADDRESS (City, State, and ZIP Code) P. O. Box 12211 Research Triangle Park, NC 27709-2211	10. SOURCE OF FUNDING NUMBERS PROGRAM ELEMENT NO. / PROJECT NO. / TASK NO. / WORK UNIT ACCESSION NO.
11. TITLE (Include Security Classification) Indentation Damage in Ceramics	
12. PERSONAL AUTHOR(S) B.R. Lawn and B.J. Hockey	
13a. TYPE OF REPORT Final 13b. TIME COVERED FROM 03/85 TO 03/87	14. DATE OF REPORT (Year, Month, Day) May 30, 1987 15. PAGE COUNT
16. SUPPLEMENTARY NOTATION The view, opinions and/or findings contained in this report are those of the author(s) and should not be construed as an official Department of the Army position, policy, or decision, unless so designated by other documentation.	

17. COSATI CODES			18. SUBJECT TERMS (Continue on reverse if necessary and identify by block number)
FIELD	GROUP	SUB-GROUP	Ceramics, Indentation, Microstructure, Strength, Wear and Machining

19. ABSTRACT (Continue on reverse if necessary and identify by block number)

The basic processes of indentation damage in brittle ceramics have been studied. Attention has focussed on the roles of material crystallography and microstructure in determining the nature of the damage pattern. Microscopy techniques, particularly transmission electron microscopy, have been used to characterize the attendant deformation and fracture of Vickers indentation sites. Strength, toughness, and wear measurements have been carried out on polycrystalline materials to ascertain how the damage characteristics influence the ensuing mechanical properties. It is concluded that material microstructure can be a crucial factor in structural design with ceramics.

20. DISTRIBUTION/AVAILABILITY OF ABSTRACT ☒ UNCLASSIFIED/UNLIMITED ☐ SAME AS RPT. ☐ DTIC USERS	21. ABSTRACT SECURITY CLASSIFICATION Unclassified
22a. NAME OF RESPONSIBLE INDIVIDUAL Brian R. Lawn	22b. TELEPHONE (Include Area Code) (301) 975-5782 22c. OFFICE SYMBOL

DD FORM 1473, 84 MAR 83 APR edition may be used until exhausted. All other editions are obsolete.

SECURITY CLASSIFICATION OF THIS PAGE
UNCLASSIFIED

END

10-87

DTIC